

# Digital-analog hybrid matrix multiplication processor for optical neural networks

Xiansong Meng<sup>1,†</sup>, Deming Kong<sup>1,†,\*</sup>, Kwangwoong Kim<sup>2</sup>, Qiuchi Li<sup>3</sup>, Po Dong<sup>4</sup>,  
Ingemar J. Cox<sup>3,5</sup>, Christina Lioma<sup>3</sup>, and Hao Hu<sup>1,\*</sup>

<sup>1</sup>DTU Electro, Technical University of Denmark, DK-2800, Kgs. Lyngby, Denmark

<sup>2</sup>Nokia Bell Labs, New Providence, NJ 07974, USA

<sup>3</sup>Department of Computer Science, University of Copenhagen, Denmark

<sup>4</sup>II-VI Incorporated, 48800 Milmont Dr., Fremont, CA 94538, USA

<sup>5</sup>Department of Computer Science, University College London, UK

<sup>†</sup>These authors contributed equally

## Corresponding authors

Correspondence to:

Deming Kong (dmkon@dtu.dk), ORCID: 0000-0001-6552-4081

Hao Hu (huhao@dtu.dk), ORCID: 0000-0002-8859-0986

## Abstract

The computational demands of modern AI have spurred interest in optical neural networks (ONNs) which offer the potential benefits of increased speed and lower power consumption. However, current ONNs face various challenges, most significantly a limited calculation precision (typically around 4 bits) and the requirement for high-resolution signal format converters (digital-to-analogue conversions (DACs) and analogue-to-digital conversions (ADCs)). These challenges are inherent to their analog computing nature and pose significant obstacles in practical implementation. Here,

we propose a digital-analog hybrid optical computing architecture for ONNs, which utilizes digital optical inputs in the form of binary words. By introducing the logic levels and decisions based on thresholding, the calculation precision can be significantly enhanced. The DACs for input data can be removed and the resolution of the ADCs can be greatly reduced. This can increase the operating speed at a high calculation precision and facilitate the compatibility with microelectronics. To validate our approach, we have fabricated a proof-of-concept photonic chip and built up a hybrid optical processor (HOP) system for neural network applications. We have demonstrated an unprecedented 16-bit calculation precision for high-definition image processing, with a pixel error rate (PER) as low as  $1.8 \times 10^{-3}$  at an signal-to-noise ratio (SNR) of 18.2 dB. We have also implemented a convolutional neural network for handwritten digit recognition that shows the same accuracy as the one achieved by a desktop computer. The concept of the digital-analog hybrid optical computing architecture offers a methodology that could potentially be applied to various ONN implementations and may intrigue new research into efficient and accurate domain-specific optical computing architectures for neural networks.

## Main

Modern artificial intelligence based on deep learning algorithms has demonstrated impressive capabilities<sup>1</sup>. However, these algorithms require enormous computing power and corresponding energy. The demand for computing power is now doubling every 3–4 months<sup>2</sup>, a rate surpassing the well-known Moore’s law. This has given rise to domain-specific hardware accelerators using application-specific integrated circuits (ASICs), for example, Google’s tensor processing units (TPUs)<sup>3</sup> and IBM’s TrueNorth<sup>4</sup>. The aim is to develop an efficient hardware platform with advanced parallelism for matrix multiplications. However, microelectronics is encountering fundamental bottlenecks in speed, energy consumption, heating, and interconnect delay, which become increasingly hard to be resolved by scaling<sup>5–7</sup>.

Photonic integrated circuits (PICs) present a pathway free from these obstacles, and hence form a promising disruptive computing architecture beyond von Neumann architecture and Moore’s Law to potentially accelerate neural network applications efficiently<sup>8–10</sup>. Consequently, integrated optical neural network (ONN) have been proposed to address the obstacles of microelectronics<sup>11,12</sup>,

showing potential to surpass their digital microelectronic counterparts in calculating speed, energy consumption, as well as computing density<sup>13</sup>. Despite the advantages of ONNs, the demonstrations are all based on analog computing architectures where the input and weight vectors (i.e., the multipliers and multiplicands for the matrix multiplication) are represented by light intensities. The analog computing nature of ONNs gives rise to a major scientific challenge: insufficient signal-to-noise ratio due to accumulated noise, and crosstalk in the computing system. This imposes several fundamental limitations. One primary limitation is the low precision of calculations. The intensity resolution of the optical signals is usually limited to a calculation precision around 4 bits<sup>14,15</sup>. Efforts have recently been made to increase the control precision of the weight values up to 9 bits for some analog ONN schemes<sup>16,17</sup>. However, this does not directly translate into a calculation precision of 9 bits for the matrix multiplication, but rather 4.2 bits based on a 99.7% confidence interval derived from the noise distribution of the obtained results<sup>17</sup>. In practice, 16-bit calculation precision is required for reasonable training convergence and many demanding inference tasks such as autonomous driving, image processing, and 3D computer vision<sup>18</sup>. Second, analog optical computing is incompatible with microelectronics, requiring high-resolution digital-to-analogue conversions (DACs) and analogue-to-digital conversions (ADCs) which are expensive and energy-consuming.

Here, we propose a new type of digital-analog hybrid matrix multiplication processor for optical neural networks. The hybrid optical processor differs fundamentally from existing analog ONN processors and offers the following benefits. The introduction of logic levels can significantly increase the calculation precision for matrix multiplication. Powerful digital signal processing (DSP) algorithms can improve calculation performance and ensure high calculation repeatability. The high-resolution DACs for the inputs can be removed; and the requirements for ADCs for the outputs can be greatly released by  $M$  bits, considering matrix-vector multiplication (MVM) of  $N$ -bit multipliers and  $M$ -bit multiplicands. In return, this can increase the operating speed and improve the compatibility with microelectronics. We propose the concept of a hybrid optical processor (HOP) in convolution neural networks. Our simulations show good noise tolerance and improved performance of the HOP over analog optical computing scheme. At an signal-to-noise ratio (SNR) of 25 dB, our HOP can achieve an root-mean-square error (RMSE) of  $1.2 \times 10^{-3}$  for an 8-bit image processing task with a  $3 \times 3$  convolutional operator. We have also built a proof-of-concept silicon

photonic chip and applied the HOP in a 16-bit depth high-definition image processing (HDIP) system, as well as handwritten digit recognition (HWDR). The convolution results show that a record high calculation precision of 16 bits is successfully achieved with a pixel error rate (PER) of  $1.8 \times 10^{-3}$  at a SNR of 18.2 dB and an operating speed of 7.5 GHz. The PER performance is also investigated under various optical noise levels for an 8-bit image processing task, showing a PER of  $6.0 \times 10^{-5}$  at an optical signal-to-noise ratio (OSNR) of 35 dB. The HWDR shows the same accuracy as the one calculated with a desktop computer. Notably, the HOP is a method that could potentially be applied to other ONN schemes and spark new concepts considering domain-specific optical computing.

## The principle of the hybrid optical processor

Analog signals are fundamentally vulnerable to noise and crosstalk. The optical computing system can be seen as an optical signal processing system and ONN is a representation of layers of the optical matrix multiplication system. Shown in Fig. 1a, analog signals traversing the signal processing system with noise and crosstalk suffer more severe degradation than digital signals under the same SNR. This is due to the absence of logic levels and decision-making processes in analog systems, which prevents the signal from being effectively recovered and equalized. The hypothesis here is that the performance of the optical computing system can benefit from the utilization of digital optical signals.

Analog optical matrix multiplication architectures rely on analog photonic multiplication cores, abstractly represented in Fig. 1b. The input  $d$  and weight  $w$  originate from M-bit and N-bit DACs in the electrical domain. After electro-optical conversion,  $d$  and  $w$  are multiplied and converted back into the electrical domain. This generates an optical signal with  $(2^M - 1) \times (2^N - 1)$  possible levels (considering signal levels starting from 0, thus  $2^M \times 2^N - 2^M - 2^N + 1$ ). To accomplish a full-precision multiplication without losing information, an ADC with a resolution (effective number of bits (ENOB)) of  $\log_2 [(2^M - 1) \times (2^N - 1)]$  bits is necessary. This can be very challenging, especially for high-speed operations, since speed-versus-resolution is a well-known trade-off for the signal converters<sup>19</sup>. While it is possible to reduce the operational speed to attain the desired resolution, the high-speed operation advantage of photonic components vanishes. On the contrary,

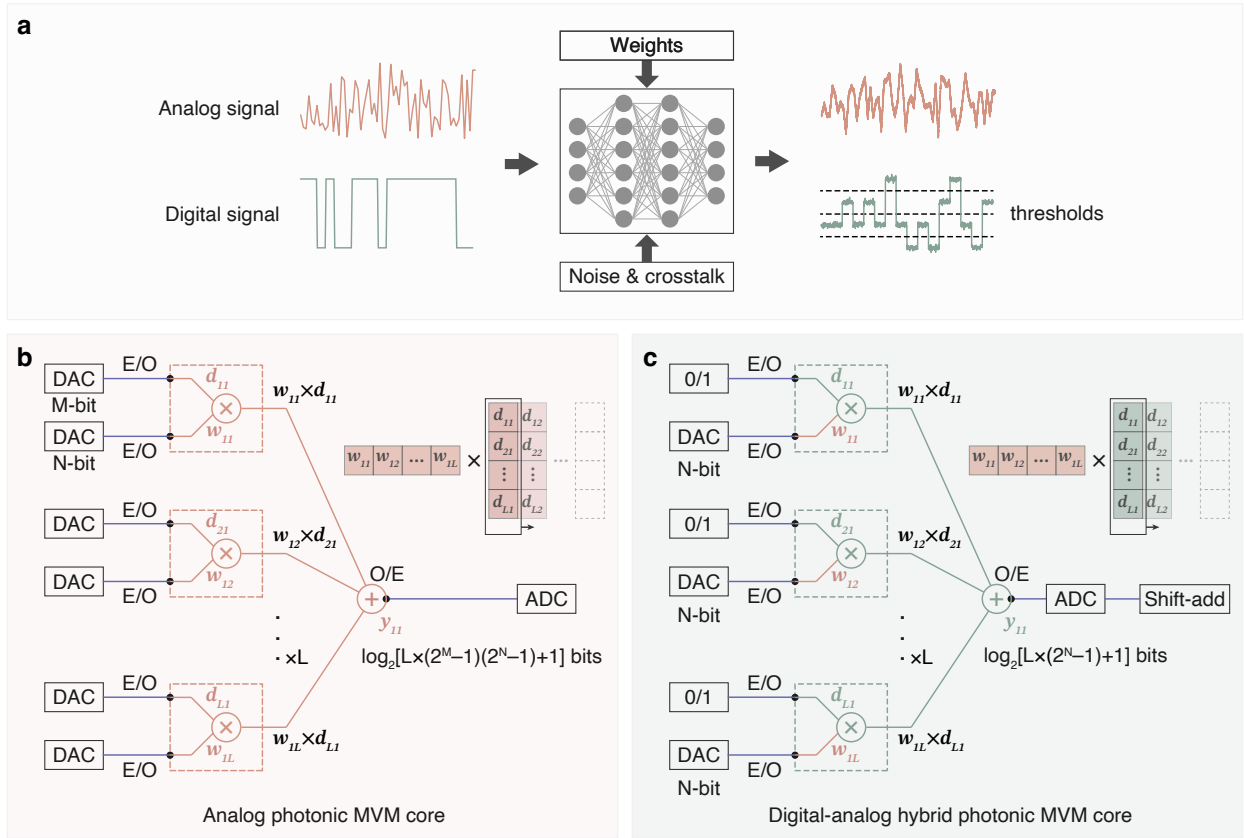


**Fig. 1 | Concept of the digital-analog hybrid photonic MVM core.** **a**, Digital signal is more robust to noise and crosstalk in a signal processing system. ONN can be seen as a signal processing system where digital signals can potentially be applied for better calculation repeatability, precision, scalability, and compatibility with microelectronics compared to analog signals. **b**, The abstracted analog photonic MVM core utilizing analog signals for both input  $d$  and weight  $w$ . **c**, The proposed digital-analog hybrid photonic MVM core utilizing digital signals for input  $d$ , with relaxed constraints for signal format converters.

while high-speed operations are maintained, the trade-off is an inevitable reduction in calculation precision (Details are discussed in Supplementary Table 1, 2 and Supplementary Figure 2). The number of overall possible signal levels increases proportionally for calculating an inner product of an input vector and a weight vector, generating  $L \times (2^M - 1) \times (2^N - 1)$  possible levels, which requires an ADC with a resolution of  $\log_2 [L \times (2^M - 1) \times (2^N - 1)]$  bits.

The HOP concept employs digital binary words for matrix multiplication into the optical computing system. For single MVM operation,  $d$  is carried in digital optical signals using binary words, while  $w$  is kept in analog format leaving the design of the computing system unchanged. If  $w$  originates from an N-bit DAC, the multiplication result is a signal with a reduced potential number of  $2^N - 1$  levels, which requires an ADC resolution of  $\log_2 (2^N - 1)$  bits. The HOP concept can be extended to build a hybrid digital-analog photonic MVM core represented in Fig. 1c. An input vector  $(d_{11}, d_{21}, \dots, d_{L1})^T$  and a weight vector  $(w_{11}, w_{12}, \dots, w_{1L})$  can be input to  $L$  multipliers. The results from the multipliers are kept in the optical domain and summed in a photo-detector. These are then processed by a post-processing electrical circuit to get the result of the vector inner product (see Supplementary Figure 1). Columns of the input matrix  $\mathbf{D}$  are loaded sequentially to accomplish the MVM operation. The vector multiplication yields  $L \times (2^N - 1)$  signal levels, requiring an ADC with a resolution of  $\log_2 [L \times (2^N - 1)]$  bits. Note that the resolution of the ADC is independent of the input vector  $d$ . In theory, the hybrid photonic MVM core can support input values of any precision without sacrificing the performance.

By eliminating the need for a high-speed DAC in processing the input matrix  $\mathbf{D}$ , the hybrid MVM core reduces costs, saves energy, and simplifies system complexity. The requirement for the resolution of ADC of the hybrid multiplier is  $\sim M$ -bit less than the analog multiplier, potentially increasing the operating speed (see Supplementary Table 1, 2 and Supplementary Figure 2). The relaxed constraints on ADC/DAC converters can improve the processor's compatibility with microelectronics. From an information encoding point of view, the analog ONN processors revolve around employing only the signal amplitude for encoding information, while the HOP utilizes both amplitude and time for information encoding. The increased encoding space in HOP results in a larger Euclidean distance between encoded signal samples when compared to analog ONN processors. As a result, the HOP has a better performance against noise and exhibit a higher calculation precision.

# An implementation of the digital-analog hybrid photonic MVM core

The HOP can be realized using microring modulator (MRM) based photonic integrated circuits. Each MRM corresponds to one hybrid photonic multiplication core, as shown in Fig. 2a. The MRM modulates a laser source of a particular wavelength. The input of the multiplier  $d$  is loaded as binary words through the high-speed ports, while the weight  $w$  from an N-bit ADC is loaded using a microheater-based modulation bias. The result is a weighted optical signal  $y$ , which is photodetected and sent to an ADC for decoding the information. The examples shown in Fig. 2 with integer inputs and weights are for illustrative purposes. The multiplier can also handle normalized decimals, where the binary words represent only the decimals. Positive and negative weights are realized by biasing the MRM at the rising and falling slope of the transmission curve (Supplementary Figure 3). The relationship between the weight and the heater bias is measured and shown in Fig. 2b. The measurement is used as a lookup table for the loading of the normalized weights. This microheater-based weight loading supports refreshing at tens of kilohertz with thermal-optic effect. However, the refresh rate of the weight vector can be much quicker if the HOP was implemented using independent input and weight loading devices, for example, based on a Mach-Zehnder modulator and an MRM array<sup>17</sup>. The HOP can therefore enable the possibility for in-situ training.

The implementation of the hybrid photonic MVM core is shown in Fig. 2c. The example illustrated here is a single  $3 \times 3$  convolution operator, but multiple convolution operators can be simultaneously integrated into a PIC to scale up for multiple convolution operations or complete matrix multiplication. A multi-wavelength light source is used with  $L$  wavelengths for the convolution with an operator of  $L$  elements. The MRM array accomplishes the element-wise multiplication of the input vector  $(d_{11}, d_{21}, \dots, d_{L1})^T$  and a weight vector (convolution operator)  $(w_{11}, w_{12}, \dots, w_{1L})$ .  $i$  denotes indices of the current column of the input matrix  $D$ . The example shows the input with 8-bit precision. The modulation generates a wavelength-division multiplexing (WDM) signal with weighted on-off keying (OOK) signaling for each wavelength (denoted as  $\lambda$ ). The results from the hybrid photonic multipliers are summed up by a photodiode, accomplishing the convolution (MVM). The photodetection results in a multilevel signal at the baseband (i.e., a pulse amplitude modulation (PAM) signal). Shown in Fig. 2d, the multilevel signal is then further processed digi-

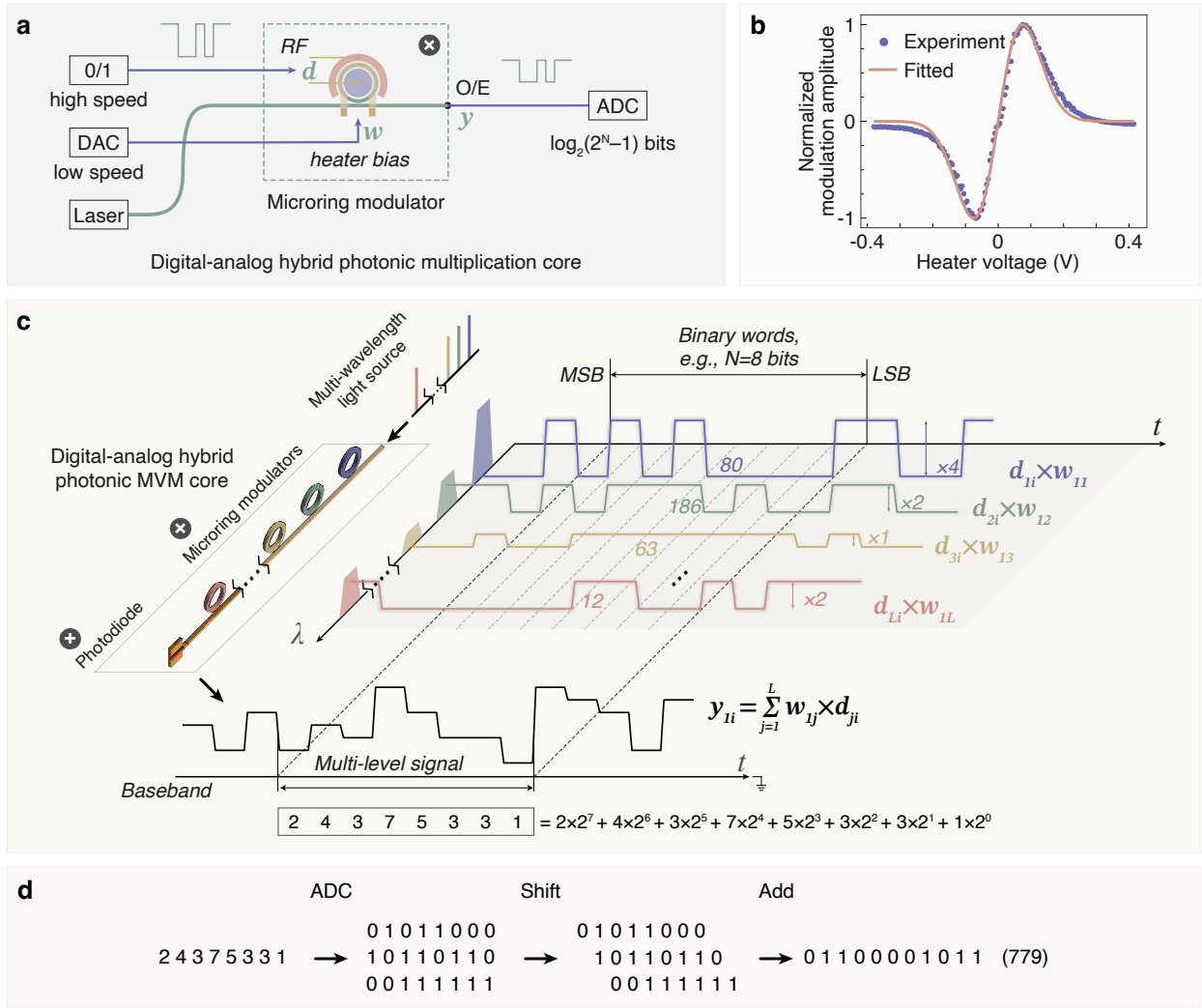


**Fig. 2 | A MRM based implementation of the hybrid digital-analog photonic MVM core.** **a**, The implementation of a single hybrid digital-analog photonic multiplication core using an MRM, where the input  $d$  in the form of a digital optical signal is loaded through the high-speed port while the weight  $w$  is loaded using microheater based modulation bias. **b**, The measured relationship between the normalized weight and the required heater voltage for the modulation bias, can be used as a lookup table to load the weight. **c**, The implementation and optical signal temporal evolution of the digital-analog hybrid photonic MVM core, including a multi-wavelength light source, an array of microring modulators, and a photodiode. **d**, Post-processing of the multilevel signal includes an ADC and a shift-add operation. Here the multilevel signal is converted to a binary signal and the final result can be recovered via shifts and adds.

tally word by word (time duration denoted as  $t_{word}$ ) by a multilevel-to-binary converter, including PAM decoding (i.e., ADC), and a shift-add operation. The multilevel-to-binary conversion process converts the final result  $y_n$  into the form of binary words (Details are discussed in Supplementary Figure 1).

## Noise tolerance and computational robustness

We explore the noise tolerance of the proposed HOP using numerical simulations with a comparison to the analog computing scheme. Figure 3a illustrates the simulation setup. An image “Chelsea” from the scikit-image dataset<sup>20</sup> is processed using the  $3 \times 3$  Prewitt convolution operator for horizontal edge detection. We apply additive white Gaussian noise to the computing systems, i.e., the weights, with a given SNR. The image has a size of  $300 \times 451$  pixels. The pixel values are normalized by feature scaling and reshaped into  $3 \times 3$  data sequences, with the current vector denoted as  $d_1 - d_9$ . The vector is multiplied with the Prewitt operator and the 9 results are summed up to form the pixel result of the processed image. For the analog scheme, the vector is encoded only on the amplitude of the signals. For the HOP scheme, the vector is encoded using binary words with 8-bit precision, representing a grey image with 8-bit color depth or 256 levels. The signal processing for the HOP scheme is done following procedures in Fig.2c,d. Finally, the resulting pixels are reassembled to present the processed image, which has a size of  $298 \times 449$ , due to the lack of padding for the boundary of the original image. Figure 3b,c give the distributions of the expected pixel values  $y$  against the processed ones  $\hat{y}$  at a SNR of 25 dB, for the analog and the HOP schemes, respectively. Insets show the processed and reconstructed images, where noisy pixels can be observed in the analog scheme, indicating a worse noise tolerance.

Figure 3d,e show the noise distribution (i.e.,  $\hat{y} - y$ ) of the output signals from the analog and the HOP schemes respectively. Results from the analog computing scheme reveal a Gaussian noise distribution with a standard deviation of 0.027. The corresponding calculation precision is 3.6 bits, calculated from the  $3\sigma$  value (99.7% confidence interval) of the Gaussian-shaped noise distribution<sup>12</sup>. The noise distribution from the results of the HOP scheme is, however, fundamentally different from the analog computing scheme due to the introduction of logic levels and decisions. The noise in the results of the HOP scheme does not comply with a Gaussian distribution. There-

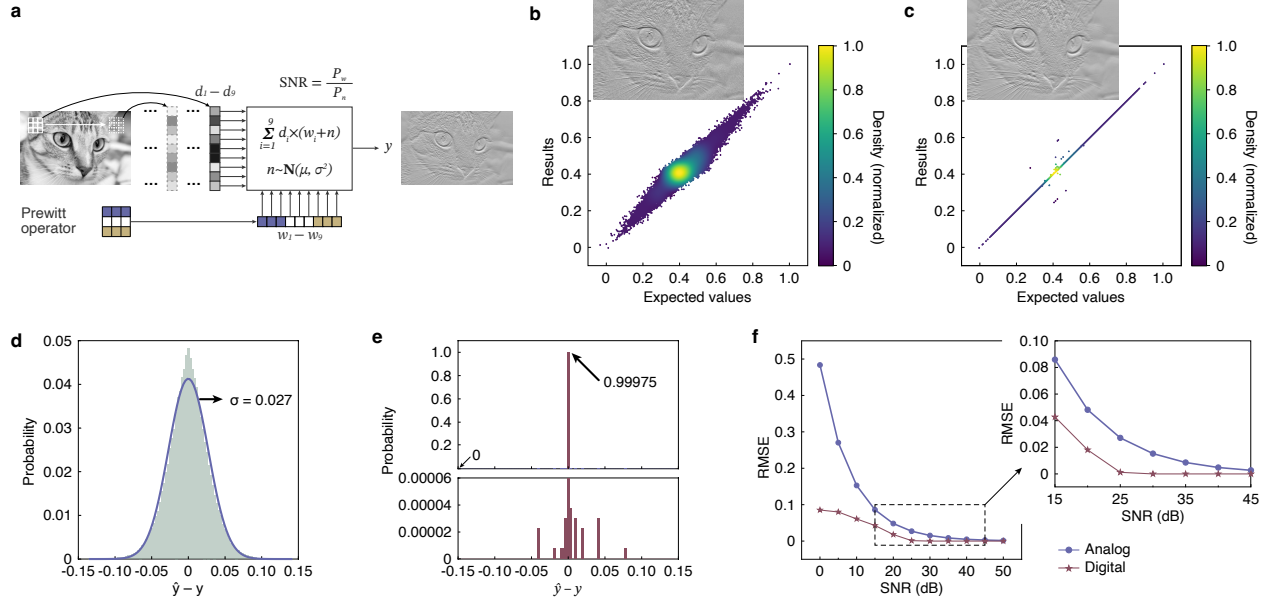


**Fig. 3 | Simulation setup and results.** **a**, Simulation setup. An image “Chelsea” from the scikit-image dataset<sup>20</sup> is convolved with a Prewitt operator (vertical edge detection). We explore the noise tolerance of both the analog and the hybrid optical computing systems by adding additive white Gaussian noise to the weights and examine the performance of the system by investigating the noise distribution of the outputs. **b,c**, Distribution of expected pixel values against the processed pixel values (both normalized) at an SNR of 25 dB, for the analog and hybrid computing systems, respectively. Insets show the corresponding processed images. Noisy pixels can be clearly observed in the image processed using analog computing. **d,e**, Noise distribution of the analog and hybrid computing systems, respectively, at an SNR of 25 dB. Analog computing reveals a Gaussian noise distribution with a standard deviation of 0.027, corresponding to a calculation precision of 3.6 bits. The HOP shows a greatly improved noise distribution thanks to the introduction of logic levels and decisions based on thresholding. **f**, performance of the analog and hybrid computing schemes in terms of RMSE with different SNRs.

fore, we borrowed the performance metrics from digital communication, i.e., error rate at a certain achievable SNR to characterize the HOP system. The PER is  $2.5 \times 10^{-4}$  at an SNR of 25 dB, realizing a calculation precision of 8 bits.

Figure 3f gives the simulation results of the RMSE against different SNRs for both computing schemes. At an SNR of 25 dB, the RMSE can be reduced from  $2.4 \times 10^{-2}$  using the analog computing scheme to  $1.2 \times 10^{-3}$  using the HOP scheme. In short, the HOP scheme outperforms its analog counterpart in noise resilience, particularly within lower SNR regimes, suggesting superior scalability potential for optical computing applications. This resilience against noise is important, considering that noise presents a significant barrier to the scalability and practical deployment of ONNs.

## Experimental setup

We demonstrate the HOP in a proof-of-concept experiment. Figure 4a shows the data loading scheme. The inputs of the HOP come from the pixel values of the “Chelsea” image. The pixel values are normalized and reshaped into  $3 \times 3$  data sequences, with the current vector denoted as  $d_1 - d_9$ . The inputs are loaded to the high-speed modulation ports of an MRM array in the form of binary words and the weights from the convolution operator are applied to the corresponding MRMs using microheater-based modulation biases. Figure 4b shows the measurement setup. The multi-wavelength light source comes from a flattened optical frequency comb (OFC) containing 9 wavelengths spaced at 80 GHz with an overall optical power of 7.0 dBm. The insets of 4b show the pictures of the packaged PIC chip and the microscopic image of the cascaded MRMs. The optical spectrum of the comb source is shown in Fig. 4c, with a central wavelength located around 1543.5 nm. An erbium-doped fibre amplifier (EDFA) with a 10-dB optical coupler and an optical spectrum analyzer (OSA) are inserted after the comb source for noise loading and OSNR evaluations. The comb source is coupled into the PIC chip of cascaded MRMs<sup>21,22</sup>. Each MRM modulates the corresponding comb line with the inputs and weights. The WDM signal generated from the MRM photonic chip is coupled into an avalanche photodiode (APD) with a launch power of  $-12.0$  dBm. The photodetected baseband multilevel signal is sampled by a digital storage oscilloscope (DSO) and is further processed by a simple DSP chain<sup>23</sup>, including low-pass filtering, resampling, and most

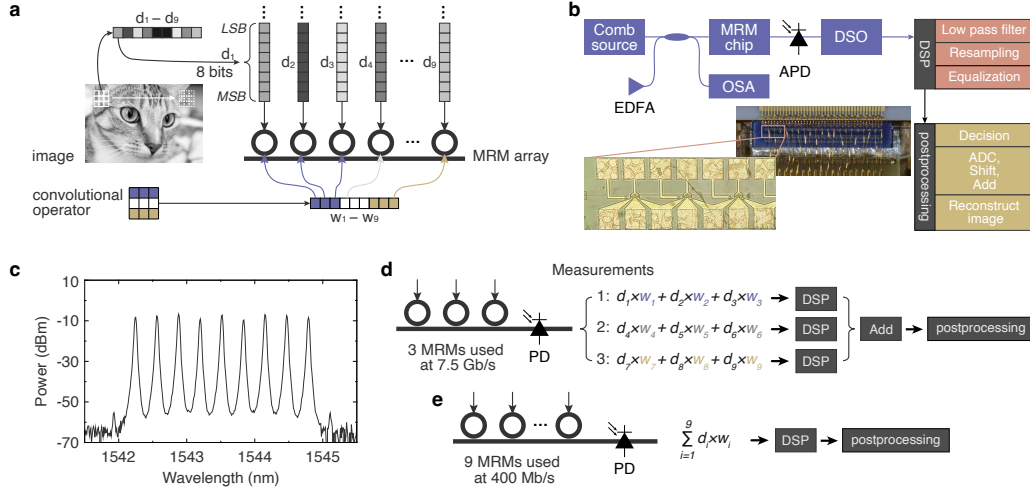


**Fig. 4 | Experimental setup.** **a**, Data loading scheme. The inputs of the HOP are the pixel values of the “Chelsea” image, used to perform the convolution operation. The inputs are loaded to the high-speed modulation ports of a set of 9 MRMs in binary words. The convolution operator is reshaped into a  $1 \times 9$  vector and applied to the same set of MRMs using microheater-based modulation biases. **b**, Measurement setup, including DSP and signal postprocessing. The HOP consists of a packaged PIC chip containing 20 cascaded MRMs, and an external photodiode (PD). Insets give the picture of the packaged chip and the microscopic image of the cascaded MRMs. **c**, The optical spectrum of the optical frequency comb source. 9 flattened comb lines are generated and fed into the MRM chip. **d**, Detailed operation condition and signal flow for the HDIP task. **e**, Detailed operation condition and signal flow for the HWDR task.

importantly equalization. Performance of the HOP is evaluated after the postprocessing procedure, including decision, multilevel-to-binary conversion (Fig. 2d), as well as image reconstruction.

To assess the performance of the HOP, we undertook two tasks, each designed to probe specific functional aspects of the system. The HDIP task is designed to evaluate the calculation precision. The HWDR task is to evaluate the HOP in an inference task by a convolutional neural network (CNN). Depicted in Fig. 4d, the HDIP task is performed with each of the MRMs working at 7.5 Gb/s. The  $3 \times 3$  convolution operator is disassembled into 3 sets and implemented through 3 measurements, due to our limited number of high-speed electrical signal channels. The results from the 3 measurements are added up together after DSP (before decision), and post-processing is done afterward for performance evaluation. Figure 4e shows the operation condition and signal flow for the HWDR task. We use an field programmable gate arrays (FPGA) for simultaneously loading 9 microring modulators at a speed of 400 Mb/s to compute the entire convolution at once.

## High-definition image processing and handwritten digit recognition

Figure 5a shows the original image and the processed red (R), Green (G), and Blue (B) channels. The image is taken from a mobile camera using uncompressed raw format. It is then converted to an image with a depth of 16 bits. The HOP processes the convolution using inputs with 16-bit binary words and applies the Prewitt vertical, Sobel vertical edge detection and Laplacian operators. The processed color channels remain in 16-bit depth and show a high-quality appearance indicating a high degree of noise resilience. This can be further proved by looking into the sequences of the pixel values with a comparison to the results calculated by a desktop computer, shown in Fig. 5b. Figure 5c shows the distribution of the expected pixel values  $y$  against the processed ones  $\hat{y}$ . Figure 5d derives the noise distribution (i.e.,  $\hat{y} - y$ ) of the results by the HOP. The corresponding measured SNR is 18.2 dB, and the PER is  $1.8 \times 10^{-3}$ . We further tested the noise tolerance of the HOP system by introducing optical noise to the multi-wavelength light source. Figure 5e gives the PER performance under tested OSNRs of the light source, for an 8-bit image processing with the Prewitt vertical operator. A PER of  $6.0 \times 10^{-5}$  is achieved at an OSNR of 35.0 dB. These results demonstrate that the HOP can handle the convolution task with very high precision, and the concept of digital-analog hybrid optical computing architecture works with a high tolerance

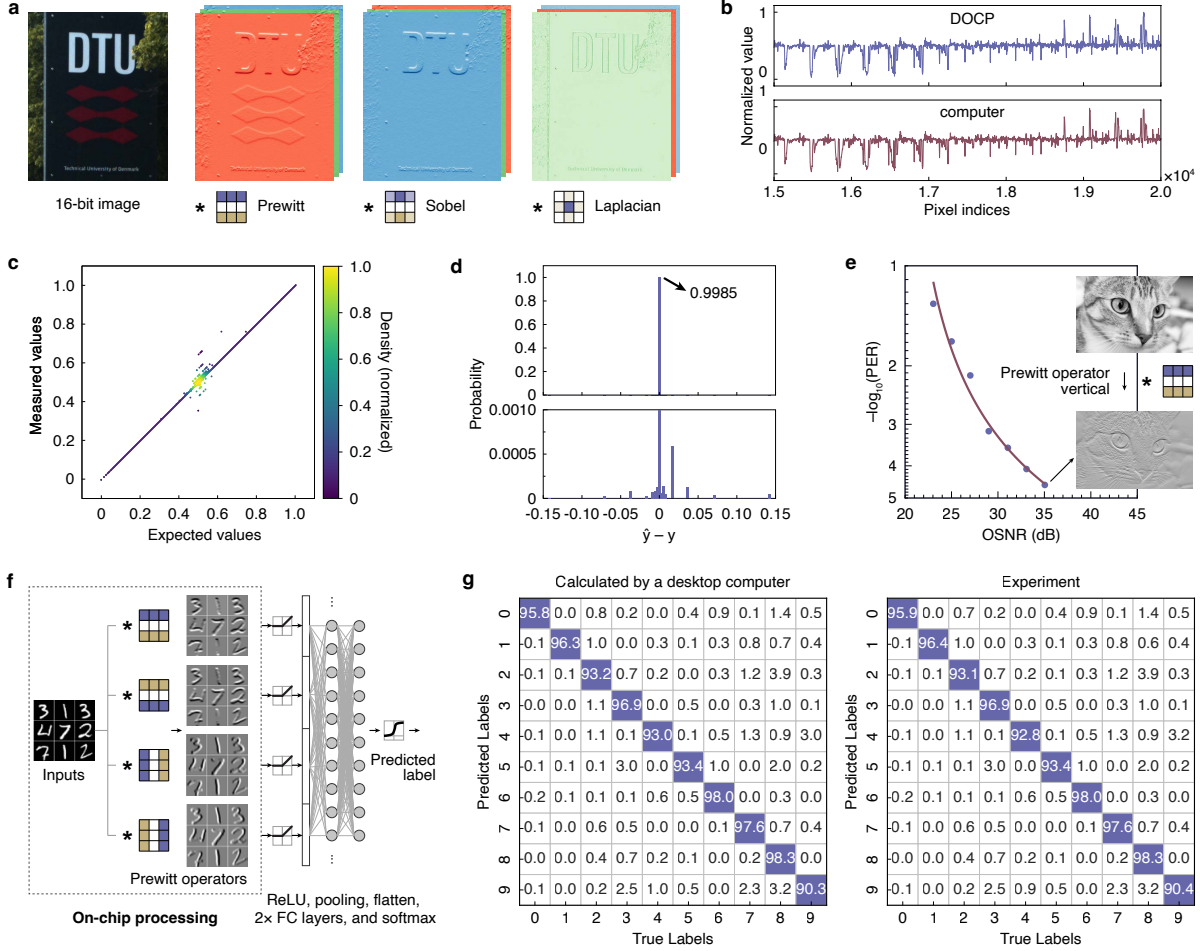


**Fig. 5 | Experiment results.** **a**, The original 16-bit image and the processed image channels using the Prewitt vertical, Sobel vertical and Laplacian operators. **b**, A section of the processed sequences of pixel values. Up: processed by the HOP; Down: processed by a desktop computer. **c**, Distribution of expected pixel values against the processed pixel values (both normalized). **d**, Noise distribution and calculation accuracy. **e**, Pixel error rate against light source OSNR. The measurements are performed on an 8-bit image processed with the Prewitt vertical operator. **f**, Layer structure of the CNN to perform the HWDR task using the modified National Institute of Standards and Technology (MNIST) database. The convolutional layer of the CNN is implemented using the HOP and the rest of the network is performed offline by a desktop computer. **g**, Confusion matrices for the prediction results, calculated by a desktop computer and the HOP.

to noise. More image results processed by different convolutional operators through HOP are demonstrated in Supplementary Figure 4.

Figure 5f presents the layer structure of the CNN used for the HWDR task, utilizing the MNIST database<sup>24</sup>. 10,000 images are processed and classified based on one convolutional layer, rectified linear unit, pooling, flatten, as well as two fully connected layers of 100 and 10 neurons. We replaced the calculation of the convolution layer using our HOP, performing a full edge detection using four Prewitt operators. Figure 5g illustrates the confusion matrices for the prediction results, calculated by a desktop computer and the HOP. We observed the same overall accuracy for the predictions compared with a desktop computer. We have also calculated the RMSEs of the 10,000 processed images compared with the true results calculated by a desktop computer. The results give a mean RMSE of  $5.4 \times 10^{-3}$  and a standard deviation of  $7.5 \times 10^{-3}$ . And the overall PER for the 10,000 images is  $2.7 \times 10^{-3}$ . The results confirm that the HOP achieves a high level of calculation precision.

## Discussion and outlook

Optical computing has evolved from digital optical logic gates for general-purpose computing<sup>25</sup> to domain-specific analog computing (for the physical implementation of neural networks<sup>11,26</sup>). Our domain-specific digital-analog hybrid optical computing architecture is conceptually different from logic-gates-based optical computing. Instead of pursuing general-purpose digital optical computing, we focus on domain-specified computing exclusively for matrix multiplications in neural networks. The implementation of matrix multiplication is based on binary modulations and linear signal processing, avoiding the nonlinear processes that are usually less efficient. Lastly, instead of pursuing an all-optical solution, the HOP combines the best of photonics for matrix multiplication and electronics for logic-level restoration. The HOP is distinctive from analog optical computing schemes for neural networks. Our results demonstrate the feasibility of overcoming the inherent challenges of analog optical computing through the digitization of optical signals. Given the benefits of better noise tolerance, the HOP has the potential to solve the obstacles of calculation precision, compatibility with microelectronics, and scaling of the ONNs (see Supplementary Table 3). Our findings here using digital optical inputs could potentially be applied to a wide range of ONN architectures,

including the Mach-Zehnder interferometer (MZI)-based coherent scheme<sup>11</sup> and diffraction-based schemes<sup>27,28</sup>.

## Methods

### The multi-wavelength light source

The multi-wavelength light source used in the experiment is an electro-optical frequency comb<sup>29,30</sup> implemented using a continuous-wave laser and optical phase modulation. An external cavity laser centered around 1543.5 nm with an output power of 10.5 dBm is launched into a phase modulator. The phase modulator is driven by a 40 GHz signal coming from a radio frequency (RF) synthesizer followed by a power amplifier. A 40-GHz spaced optical frequency comb is generated and fed into a wavelength-selective switch (WSS) after amplification. It is line-by-line filtered and equalized by the WSS, generating a flattened optical frequency comb with 9 comb lines and an amplitude variation of 1 dB. The amplitude variation is not calibrated nor compensated for the computing system due to the noise tolerance of the HOP. In principle, compensating for residual system impairments, like the amplitude variation within the optical frequency comb, could further enhance the HOP's performance.

### The microring modulator array chip

The PIC chip contains 20 cascaded MRMs, with a spacing of 250  $\mu\text{m}$  between adjacent MRMs. Each MRM has a ring radius of 7.5  $\mu\text{m}$ , thus a free spectral range around 13.1 nm. A microheater is sitting on top of each MRM for the alignment of the wavelength channels and the control of the modulation biases. The MRMs are based on a reverse-biased P-N junction in the middle of the microring waveguide<sup>22,31</sup>. The PIC chip is fabricated on a standard silicon-on-insulator wafer with a top silicon thickness of 220 nm. It is packaged with two edge coupling fibers, a high-speed printed circuit board (PCB) supporting 20 high-speed transmission lines, and a second PCB for the control of the microheaters. The electro-optical modulation bandwidth of the packaged modulators is measured to be around 15 GHz.

## The signal source and digital signal processing

In the HDIP task, an arbitrary waveform generator (AWG) (Keysight M8195A) is used. Limited by the available channels, 3 measurements are consecutively carried out. Each measurement uses 3 channels from the AWG at a speed of 7.5 Gb/s and a sampling rate of 15 GSa/s. The speed and the sampling rate are limited due to the use of external memory to load the entire image data, thus a mandatory clock division of four. In the HWDR task, an FPGA board (Xilinx ZCU104) is used to generate the 9 inputs to the HOP. The data rate for each data channel is set to 400 Mb/s due to the limitation of the direct memory access module.

The weighted WDM signal is detected by an APD with a 3-dB bandwidth of 10 GHz. The photodetected baseband multilevel signal is sampled by a DSO (Agilent DSA-X 93304Q) with a sampling rate of 80 GSa/s and an analog bandwidth of 33 GHz. The samples are processed offline using DSP algorithms. We use a  $T/2$ -spaced linear feedforward equalizer with a filter length of 51 to compensate for the linear impairments from the devices used in the experiment, including the RF components, the high-speed PCB board, the PIC chip, as well as the APD. The coefficients of the equalizer are obtained through training based on the least-mean-square algorithm.

## Data Availability

Source data are provided with this paper. The measurement data generated in this study and processing scripts have also been deposited in <https://doi.org/10.5281/zenodo.10026199>.

## Code Availability

The algorithms used for the data loading, reconstructions, and digital signal processing are standard and are outlined in detail in the Methods. Python scripts can be provided by the corresponding authors upon reasonable request.

## References

- [1] Wu, T. *et al.* A brief overview of chatgpt: The history, status quo and potential future development. *IEEE/CAA Journal of Automatica Sinica* **10**, 1122–1136 (2023).

- [2] Amodei, D. & Hernandez, D. Review of ai and compute. <https://openai.com/blog/ai-and-compute/> (2018).
- [3] Jouppi, N. P. *et al.* In-datacenter performance analysis of a tensor processing unit. In *Proceedings of the 44th annual international symposium on computer architecture*, 1–12 (2017).
- [4] Merolla, P. A. *et al.* A million spiking-neuron integrated circuit with a scalable communication network and interface. *Science* **345**, 668–673 (2014).
- [5] Theis, T. N. & Wong, H.-S. P. The end of moore’s law: A new beginning for information technology. *Computing in Science Engineering* **19**, 41–50 (2017).
- [6] Rupp, K. *et al.* 42 years of microprocessor trend data. <https://www.kartrupp.net/2018/02/42-years-of-microprocessor-trend-data/> [Online] (2018).
- [7] Khan, H. N., Hounshell, D. A. & Fuchs, E. R. Science and research policy at the end of moore’s law. *Nature Electronics* **1**, 14–21 (2018).
- [8] Caulfield, H. J. & Dolev, S. Why future supercomputing requires optics. *Nature Photonics* **4**, 261–263 (2010).
- [9] Miller, D. A. B. Perfect optics with imperfect components. *Optica* **2**, 747–750 (2015).
- [10] Peng, H.-T., Nahmias, M. A., de Lima, T. F., Tait, A. N. & Shastri, B. J. Neuromorphic photonic integrated circuits. *IEEE Journal of Selected Topics in Quantum Electronics* **24**, 1–15 (2018).
- [11] Shen, Y. *et al.* Deep learning with coherent nanophotonic circuits. *Nature Photonics* **11**, 441–446 (2017).
- [12] Feldmann, J. *et al.* Parallel convolutional processing using an integrated photonic tensor core. *Nature* **589**, 52–58 (2021).
- [13] Nahmias, M. A. *et al.* Photonic multiply-accumulate operations for neural networks. *IEEE Journal of Selected Topics in Quantum Electronics* **26**, 1–18 (2019).
- [14] Tait, A. N., De Lima, T. F., Nahmias, M. A., Shastri, B. J. & Prucnal, P. R. Multi-channel control for microring weight banks. *Optics Express* **24**, 8895–8906 (2016).

- [15] Tait, A. N. *et al.* Neuromorphic photonic networks using silicon photonic weight banks. *Scientific reports* **7**, 1–10 (2017).
- [16] Zhang, W. *et al.* Silicon microring synapses enable photonic deep learning beyond 9-bit precision. *Optica* **9**, 579–584 (2022).
- [17] Bai, B. *et al.* Microcomb-based integrated photonic processing unit. *Nature Communications* **14**, Article number: 66 (2023).
- [18] Gupta, S., Agrawal, A., Gopalakrishnan, K. & Narayanan, P. Deep learning with limited numerical precision. In *International conference on machine learning*, 1737–1746 (PMLR, 2015).
- [19] Murmann, B. ADC Performance Survey 1997-2023. [Online]. Available: <https://github.com/bmurmann/ADC-survey>.
- [20] Van der Walt, S. *et al.* scikit-image: image processing in python. *PeerJ* **2**, e453 (2014).
- [21] Kong, D. *et al.* Intra-datacenter interconnects with a serialized silicon optical frequency comb modulator. *Journal of Lightwave Technology* **38**, 4677–4682 (2020).
- [22] Dong, P., Lee, J., Kim, K., Chen, Y.-K. & Gui, C. Ten-channel discrete multi-tone modulation using silicon microring modulator array. In *2016 Optical Fiber Communications Conference and Exhibition (OFC)*, 1–3 (2016).
- [23] Kong, D. *et al.* 100 Gbit/s PAM-16 Transmission in the 2- $\mu$ m Band over a 1.15-km Hollow-Core Fiber. In *Optical Fiber Communications Conference (OFC) 2021*, Th4E.6 (IEEE, 2021).
- [24] LeCun, Y., Cortes, C. & Burges, C. J. The MNIST database of handwritten digits. [Online]. Available: <http://yann.lecun.com/exdb/mnist/>.
- [25] Bogoni, A., Wu, X., Bakhtiari, Z., Nuccio, S. & Willner, A. E. 640 gbits/s photonic logic gates. *Opt. Lett.* **35**, 3955–3957 (2010).
- [26] Xingyuan, X. *et al.* 11 TOPS photonic convolutional accelerator for optical neural networks. *Nature* **589**, 44–51 (2021).

- [27] Luo, X. *et al.* Metasurface-enabled on-chip multiplexed diffractive neural networks in the visible. *Light: Science & Applications* **11**, Article number: 158 (2022).
- [28] Luo, Y. *et al.* Design of task-specific optical systems using broadband diffractive neural networks. *Light: Science & Applications* **8**, Article number: 112 (2019).
- [29] Parriaux, A., Hammani, K. & Millot, G. Electro-optic frequency combs. *Adv. Opt. Photon.* **12**, 223–287 (2020).
- [30] Kong, D. *et al.* Cavity-less sub-picosecond pulse generation for the demultiplexing of a 640 Gbaud OTDM signal. In *IEEE Photonics Conference (IPC) 2015*, WG1.2 (IEEE, 2015).
- [31] Dong, P. *et al.* Wavelength-tunable silicon microring modulator. *Opt. Express* **18**, 10941–10946 (2010).

## Acknowledgements

D.K. acknowledges the research grant (VIL53077) of the Young Investigator Program (DONN) from the VILLUM FONDEN. H.H. acknowledges the research grant (VIL34320) of the Synergy Program (Searchlight) from the VILLUM FONDEN.

## Author Contributions Statement

X.M. and D.K. conceived the concept and the experiment; X.M. and Q.L. performed the simulations, supervised by D.K., I.C. and C.L.; D.K. and X.M. designed the experiment; X.M. and D.K. constructed the experiment setup, performed the experiment, and processed the data; P.D. designed the PIC; K.K. packaged the PIC; D.K. and X.M. characterized the PIC; X.M., D.K., I.C., C.L. and H.H. discussed the results; The manuscript was written by D.K. and X.M., and all authors contributed to the writing; D.K. and H.H. supervised the projects.

## Competing Interests Statement

The authors declare no competing interests.

## Figure Legends

**Fig. 1 | Concept of the digital-analog hybrid photonic MVM core.** **a**, Digital signal is more robust to noise and crosstalk in a signal processing system. ONN can be seen as a signal processing system where digital signals can potentially be applied for better calculation repeatability, precision, scalability, and compatibility with microelectronics compared to analog signals. **b**, The abstracted analog photonic MVM core utilizing analog signals for both input  $d$  and weight  $w$ . **c**, The proposed digital-analog hybrid photonic MVM core utilizing digital signals for input  $d$ , with relaxed constraints for signal format converters.

**Fig. 2 | A MRM based implementation of the digital-analog hybrid photonic MVM core.** **a**, The implementation of a single hybrid digital-analog photonic multiplication core using an MRM, where the input  $d$  in the form of a digital optical signal is loaded through the high-speed port while the weight  $w$  is loaded using microheater based modulation bias. **b**, The measured relationship between the normalized weight and the required heater voltage for the modulation bias, can be used as a lookup table to load the weight. **c**, The implementation and optical signal temporal evolution of the digital-analog hybrid photonic MVM core, including a multi-wavelength light source, an array of microring modulators, and a photodiode. **d**, Post-processing of the multi-level signal includes an ADC and a shift-add operation. Here the multilevel signal is converted to a binary signal and the final result can be recovered via shifts and adds.

**Fig. 3 | Simulation setup and results.** **a**, Simulation setup. An image “Chelsea” from the scikit-image dataset<sup>20</sup> is convolved with a Prewitt operator (vertical edge detection). We explore the noise tolerance of both the analog and the hybrid optical computing systems by adding additive white Gaussian noise to the weights and examine the performance of the system by investigating the noise distribution of the outputs. **b,c**, Distribution of expected pixel values against the processed pixel values (both normalized) at an SNR of 25 dB, for the analog and hybrid computing systems, respectively. Insets show the corresponding processed images. Noisy pixels can be clearly observed in the image processed using analog computing. **d,e**, Noise distribution of the analog and hybrid computing systems, respectively, at an SNR of 25 dB. Analog computing reveals a Gaussian noise

distribution with a standard deviation of 0.027, corresponding to a calculation precision of 3.6 bits. The HOP shows a greatly improved noise distribution thanks to the introduction of logic levels and decisions based on thresholding. **f**, performance of the analog and hybrid computing schemes in terms of RMSE with different SNRs.

**Fig. 4 | Experimental setup.** **a**, Data loading scheme. The inputs of the HOP are the pixel values of the “Chelsea” image, used to perform the convolution operation. The inputs are loaded to the high-speed modulation ports of a set of 9 MRMs in binary words. The convolution operator is reshaped into a  $1 \times 9$  vector and applied to the same set of MRMs using microheater-based modulation biases. **b**, Measurement setup, including DSP and signal postprocessing. The HOP consists of a packaged PIC chip containing 20 cascaded MRMs, and an external PD. Insets give the picture of the packaged chip and the microscopic image of the cascaded MRMs. **c**, The optical spectrum of the optical frequency comb source. 9 flattened comb lines are generated and fed into the MRM chip. **d**, Detailed operation condition and signal flow for the HDIP task. **e**, Detailed operation condition and signal flow for the HWDR task.

**Fig. 5 | Experiment results.** **a**, The original 16-bit image and the processed image channels using the Prewitt vertical, Sobel vertical and Laplacian operators. **b**, A section of the processed sequences of pixel values. Up: processed by the HOP; Down: processed by a desktop computer. **c**, Distribution of expected pixel values against the processed pixel values (both normalized). **d**, Noise distribution and calculation accuracy. **e**, Pixel error rate against light source OSNR. The measurements are performed on an 8-bit image processed with the Prewitt vertical operator. **f**, Layer structure of the CNN to perform the HWDR task using the MNIST database. The convolutional layer of the CNN is implemented using the HOP and the rest of the network is performed offline by a desktop computer. **g**, Confusion matrices for the prediction results, calculated by a desktop computer and the HOP.

# Digital-analog hybrid matrix multiplication processor for optical neural networks

## Supplementary Information

Xiansong Meng<sup>1,†</sup>, Deming Kong<sup>1,†,\*</sup>, Kwangwoong Kim<sup>2</sup>, Qiuchi Li<sup>3</sup>, Po Dong<sup>4</sup>,  
Ingemar Cox<sup>3</sup>, Christina Lioma<sup>3</sup>, and Hao Hu<sup>1,\*</sup>

<sup>1</sup>DTU Electro, Technical University of Denmark, DK-2800, Kgs. Lyngby, Denmark

<sup>2</sup>Nokia Bell Labs, New Providence, NJ 07974, USA

<sup>3</sup>Department of Computer Science, University of Copenhagen, Denmark

<sup>4</sup>II-VI Incorporated, 48800 Milmont Dr., Fremont, CA 94538, USA

<sup>†</sup>These authors contributed equally

### Corresponding authors

Correspondence to:

Deming Kong (dmkon@dtu.dk), ORCID: 0000-0001-6552-4081

Hao Hu (huhao@dtu.dk), ORCID: 0000-0002-8859-0986

## 1 Post-processing circuit for the hybrid optical processor

The post-processing converts the multi-level signal into the final calculation result and can be implemented using microelectronic circuits. We use an 8-bit wide calculated result as an example in the following discussion. The output of the hybrid optical processor (HOP) is a pulse amplitude modulation (PAM)-like signal. It is decoded and further converted into parallel 8-bit digital sequences by a high-speed analogue-to-digital conversion (ADC), as depicted in Supplementary Figure 1a, b. The high-speed digital sequences are then transformed into low-speed digital binaries

using a deserializer. For instance, a single output sequence of the ADC with a clock speed of 7.5 GHz can be down-converted to 1/8 speed through a deserializer, i.e., to a speed of 937.5 MHz, as shown in Supplementary Figure 1c. The deserializing process facilitates subsequent electrical circuits. The converted data are then routed to a logic circuit, as shown in Supplementary Figure 1d, which resolves the final calculated result. This circuitry works similarly to an 8-bit multiplier, including a number of half-adders and full-adders, but without AND gates preceding the adders. Although the circuit can introduce some gate latency, as illustrated in Supplementary Figure 1e, the whole post-processing can be accomplished in a single electrical clock cycle.

## 2 Detailed comparison between the hybrid optical processor and analog computing schemes

We show theoretically the computing power of the HOP and compare it with analog optical computing schemes in the following discussions. As previously discussed in the paper (see Figure 1b and 1c), the output signals of both schemes are processed by the ADCs and the resolution (effective number of bits (ENOB)) requirement are as follows:

$$\text{ENOB}_{\text{Analog}} = \log_2 [L \times (2^M - 1) \times (2^N - 1)] \quad (1)$$

$$\text{ENOB}_{\text{Hybrid}} = \log_2 [L \times (2^N - 1)] \quad (2)$$

where M and N denote the resolution (bit widths) of input data 'd' and weight value 'w', respectively; L is the number of multiplications for the inner product of the input (multiplicand) vector and the weight (multiplier) vector, representing the scale of the convolutional operator and optical hardware. Given that the input in the hybrid scheme is binary data, 'M' equals 1. The required ENOB of the ADC increases with the scale of the weight vector and the bit width of each single weight in both schemes. Yet, the required ENOB for the analog scheme also increases with the bit width of the inputs. This means that, with the same hardware scale, the required ENOB of the analog scheme surpasses its counterpart in the HOP scheme when the bit width of the inputs is greater than 2.

However, it is known in practice<sup>1</sup> that the maximum sampling rate of the ADC is inversely



proportional to  $2^{\text{ENOB}}$

$$F_s = \frac{c}{2^{\text{ENOB}}} \quad (3)$$

where  $c$  is a constant, with a typical value of 5 TS/s-levels for cutting-edge ADCs implementations. Utilizing equations (1) and (2), the maximum sampling rate (i.e., the speed of operations) to ensure a certain calculation precision for both the analog and hybrid computing schemes can be calculated. We can see that the achievable sampling rate of the ADC is inversely proportional to the scale for a single convolutional operator.

$$F_s(\text{Analog}) = \frac{5}{L \times (2^M - 1) \times (2^N - 1)} \text{ TS/s} \quad (4)$$

$$F_s(\text{Hybrid}) = \frac{5}{L \times (2^N - 1)} \text{ TS/s} \quad (5)$$

Then the computing power  $P$  for a single operator in terms of tera operations per second (TOPS) for two schemes can be further calculated by multiplying the hardware scale (i.e.,  $L$ ) with the maximum achievable speed of the system (proportional to the sampling rate of the ADCs, i.e.,  $F_s$ ), shown as equations (6) and (7).

$$P_{\text{Analog}} \propto \frac{5}{(2^M - 1) \times (2^N - 1)} \text{ TOPS} \quad (6)$$

$$P_{\text{Hybrid}} \propto \frac{5}{p \times (2^N - 1)} \text{ TOPS} \quad (7)$$

where  $p$  is the bit width (precision) of the binary inputs and the multi-level outputs.

For the analog computing scheme, we have assumed that the digital-to-analogue conversions (DACs) will not impose any speed or precision limit. Therefore, the computing speed is determined by the achievable operating speed of the ADCs. In practice, the performance of the analog computing scheme is also limited by the DACs. This assumption here is used for simplicity reasons only, thus the calculated performance for the analog scheme is overestimated.

For the hybrid computing scheme, no DACs is used. But the input data is binary words with  $p$ -bit precision, thus  $p$  times slower than the analog scheme, in theory. For example, if we assume 8-bit input data with a clock rate of 10 GHz for both the analog scheme using DACs and the hybrid

scheme using pattern generators (0s and 1s), then the input rate for binary words in the hybrid scheme is divided by 8, i.e., 1.25 GHz.

A major conclusion can be drawn from equations (6) and (7). The computing power, TOPS, does not scale with the size for a single convolutional operator. Along with the increase in the scale of the hardware (i.e.,  $L$ ), the requirement for ENOB is increased, leading to a reduction of the sampling rate of the ADC (equation (4) and (5)). The hardware scale  $L$  is eventually canceled out in the TOPS. This also indicates that the ADCs are the main bottlenecks of the computing systems, both for the analog scheme and the hybrid scheme. Note that this conclusion should not only apply to photonic computing schemes but also to microelectronics-based analog computing.

To overcome this, one can implement multiple operators to increase the overall computing power for the whole computing system. In other words, multiple low-resolution ADCs can be utilized together with small-scale operators (resulting in fewer signal levels and thus possible higher ADC sampling rate), instead of a large matrix-vector multiplication (MVM) operator with a high-resolution ADC. The study of ADC<sup>1</sup> demonstrates that the requirement for logic gate resources increases exponentially with the resolution of the ADC. Therefore, deploying multiple low-resolution ADCs consumes a similar amount of logic gate resources as a single high-precision ADCs.

The above approach could increase the sampling rate of the ADCs without sacrificing the overall electrical hardware resource, thus achieving a higher computing power of the computing system. Therefore, the HOP is particularly well-suited for processing tasks that require a large number of small convolutional operators, such as the widely-known object detection model, You Only Look Once (YOLO)<sup>2</sup>.

However, it should be noted that the hybrid scheme can have some advantage over the analog scheme in terms of speed and computing power, according to equations (4), (5), (6), and (7). To quantitatively compare the two schemes, we assume a convolution task with an operator of size  $3 \times 3$ . It is assumed that the input data 'd', transmitted through a high-speed DAC or pattern generator, has a rate of 40 GHz with precision ranging from 1 bit to 8 bit. The weight has a precision of 8 bit. Employing the equations and assuming an input data rate of 40 GHz, we can calculate the required ENOB of the ADCs (equation (1) and (2)), achievable ADC sampling rate in theory (equation (4) and (5)), and the TOPS (equation (6) and (7)). These results are presented in Table 1 and Table 2.

Input Data Precision	1 bit	2 bit	3 bit	4 bit	5 bit	6 bit	7 bit	8 bit
Required ADC ENOB	3.3 bit	6.4 bit	8.8 bit	11 bit	13.1 bit	15.1 bit	17.1 bit	19.2 bit
ADC Achievable Speed	500 GHz	60.9 GHz	11.3 GHz	2.5 GHz	578 MHz	140 MHz	34.4 MHz	8.5 MHz
DAC Speed	40 GHz	40 GHz	40 GHz	40 GHz	40 GHz	40 GHz	40 GHz	40 GHz
System Speed <sup>1</sup>	40 GHz	40 GHz	11.3 GHz	2.5 GHz	578 MHz	140 MHz	34.4 MHz	8.5 MHz
TOPS <sup>2</sup>	3.6E-1	3.6E-1	1E-1	2.2E-2	5.2E-3	1.2E-3	3.1E-4	8E-5

**Supplementary Table 1** | TOPS performance of analog optical processor with various different calculation precision levels.

<sup>1</sup> The system speed is determined by the lesser of two speeds: the maximum achievable speed of the ADC and the input data speed through the DAC.

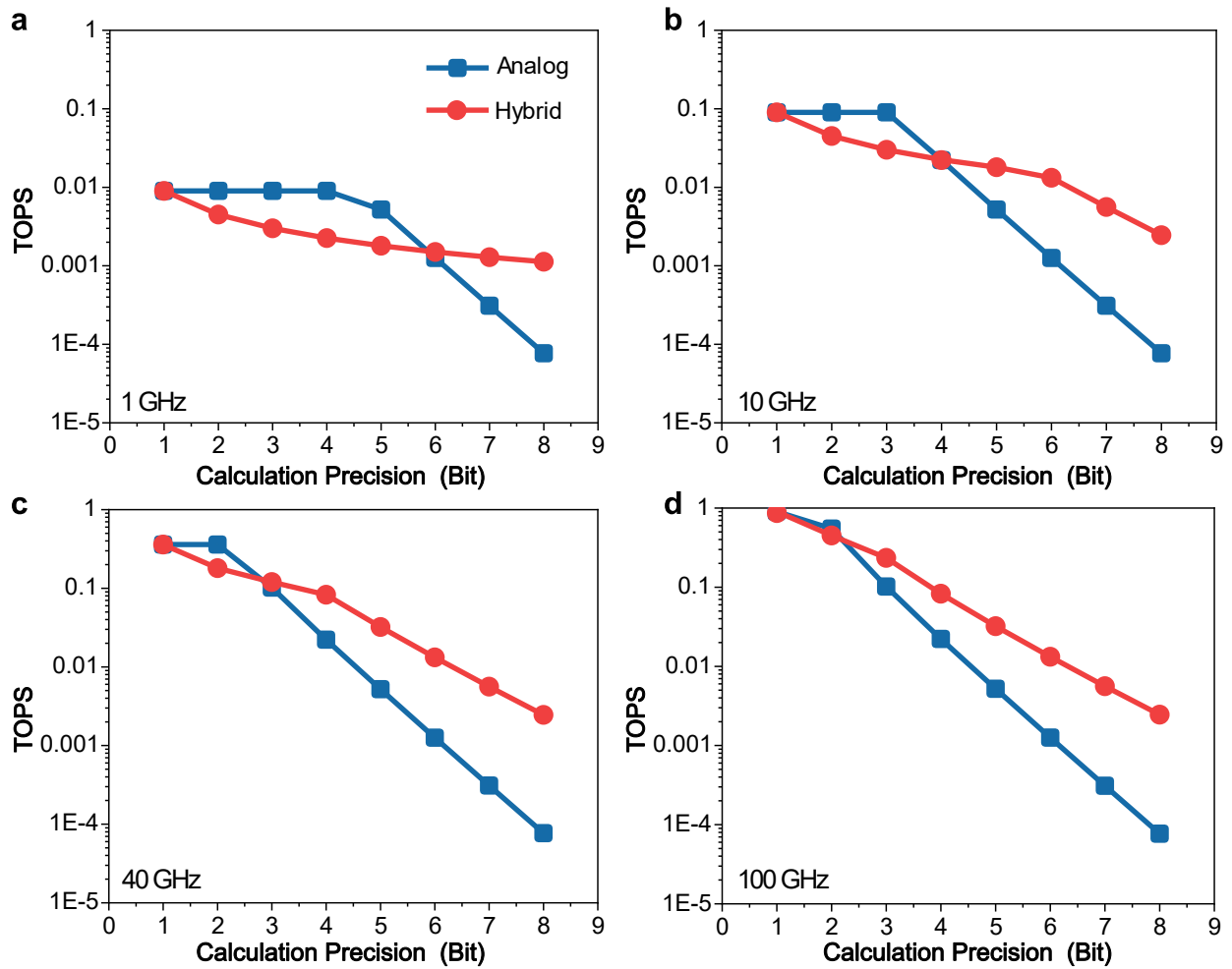
<sup>2</sup> The convolution task utilizes a  $3 \times 3$  size kernel, and the weight value precision is 8 bit. The TOPS is calculated by multiplying the hardware scale (i.e.,  $L = 9$ ) with the speed of the system.

The computing power for both the analog scheme and the HOP scheme are further illustrated in Supplementary Figure 2c. It is evident that for both the analog and hybrid schemes, the TOPS decreases as the calculation precision increases. Notably, an intersection occurs at 3-bit calculation precision. This indicates that the analog scheme holds an advantage in computing power at low-bit precision. However, the hybrid scheme demonstrates better performance with higher precision.

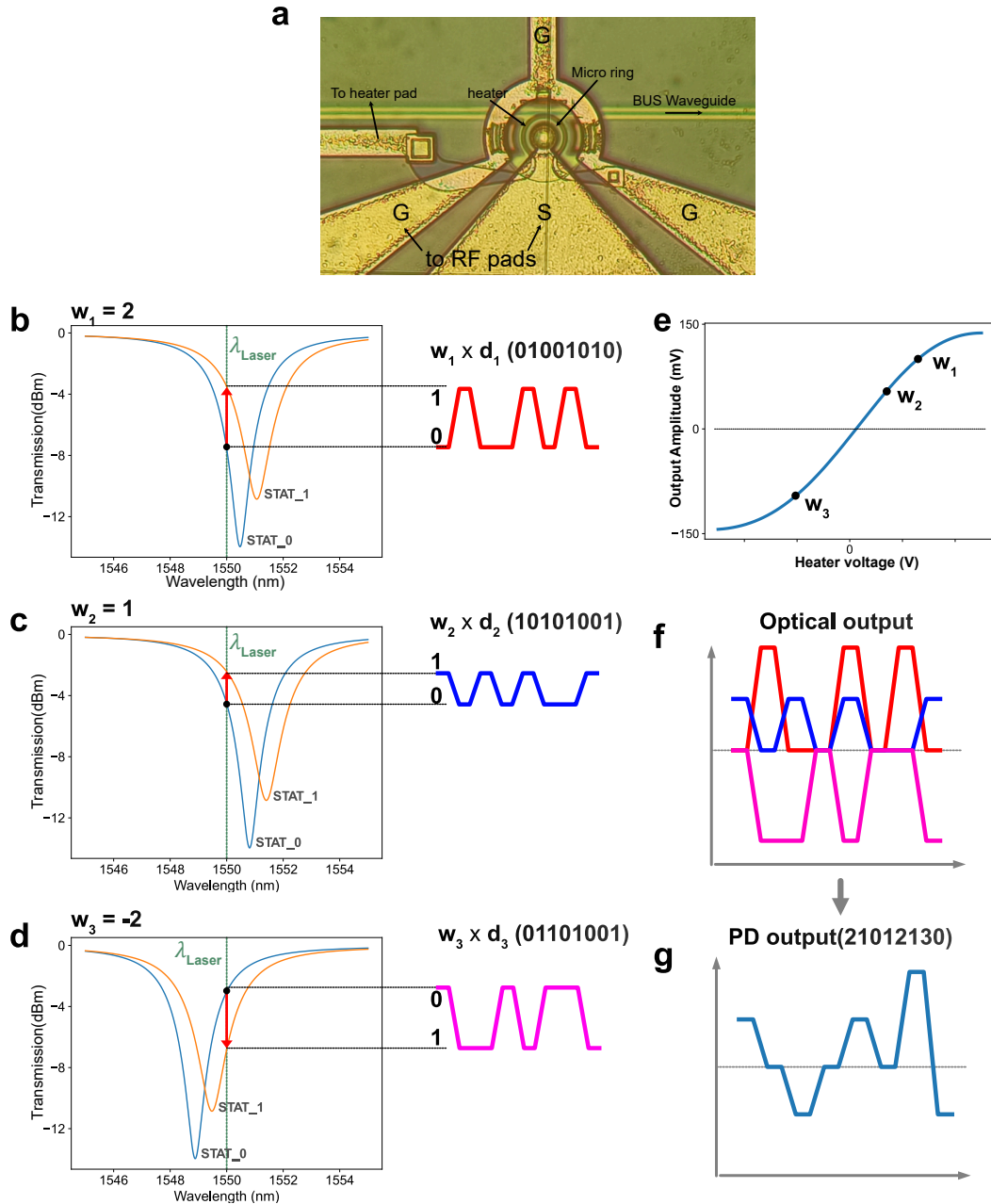
We also explore various other input rates, including 1 GHz, 10 GHz, and 100 GHz, as shown in Supplementary Figure 2a,b, and d. With higher input rates, the advantage in TOPS by the hybrid scheme gets bigger and the analog scheme gradually loses its advantage at low calculation precision regions.

### 3 Detailed weight loading and MRM modulation bias tuning

The detailed weight loading scheme for the photonic multiplier based on the MRM is shown in Supplementary Figure 3. We plot the working status, i.e., transmission curve, of the MRM when loading weight values of 2, 1, and -2, respectively, in Supplementary Figure 3b-d. The blue and



Supplementary Figure 2 | The computing power of analog and hybrid schemes: a comparison across various calculation precisions (from 1-bit to 8-bit) and input data speeds (1 GHz, 10 GHz, 40 GHz and 100 GHz).



**Supplementary Figure 3 | Detailed weight loading and microring modulator (MRM) modulation bias tuning.** **a**, Top-view microscope image of a single MRM. **b-d**, MRM working status at weight value  $w = 2$ ,  $w = 1$ , and  $w = -2$ , respectively. **e**, The relation between heater voltage and amplitude of the photodetected multiplication result. **f-g**, The addition of multi-wavelength optical signals results in a multilevel digital signal at the baseband representing the inner product of the input vector  $d$  and weight vector  $w$ . Note the zero voltage level does not necessarily correspond to the minimum level of the baseband multilevel digital signal.

Input Data Precision	1 bit	2 bit	3 bit	4 bit	5 bit	6 bit	7 bit	8 bit
Required ADC ENOB	3.3 bit	4.8 bit	6.0 bit	7.1 bit	8.1 bit	9.1 bit	10.2 bit	11.2 bit
ADC Achievable Speed	500 GHz	178 GHz	78 GHz	36.8 GHz	17.9 GHz	8.8 GHz	4.4 GHz	2.2 GHz
Digital I/O Speed	40 GHz	40 GHz	40 GHz	40 GHz	40 GHz	40 GHz	40 GHz	40 GHz
System Speed <sup>1</sup>	40 GHz	40 GHz	40 GHz	36.8 GHz	17.9 GHz	8.8 GHz	4.4 GHz	2.2 GHz
TOPS <sup>2</sup>	4.5E-2	4.5E-2	4.5E-2	4.1E-2	2E-2	9.9E-3	4.9E-3	2.5E-3

**Supplementary Table 2** | TOPS performance of hybrid optical processor with various different calculation precision levels.

<sup>1</sup> The system speed is determined by the lesser of two speeds: the maximum achievable speed of the ADC and the input data speed through the digital I/O.

<sup>2</sup> The convolution task utilizes a  $3 \times 3$  size kernel, and the weight value precision is 8 bit. The TOPS is calculated by multiplying the hardware scale (i.e.,  $L = 9$ ) with the speed of the system, and then dividing by the bit depth of input data, in accordance with the working principle of HOP.

orange curves indicate the 'off' operating status (STAT\_0) and the 'on' operating status (STAT\_1) of the MRM. The amplitude of the output is determined by the optical intensity difference between these two statuses, which can be adjusted by tuning the applied voltage on the microheater, i.e., the working wavelength of the MRM. In other words, the weight of the multiplier is adjusted by tuning the voltage applied to the microheater. Positive and negative weight values can both be realized by tuning the initial working wavelength of the MRM. If the initial working wavelength resides on the red side (longer wavelengths) of the laser wavelength, positive weight values can be loaded. On the contrary, an initial working wavelength at the blue side of the laser wavelength will result in a flip of logic 0 and 1, thus a negative weight value is loaded.

The relationship between the weight and the microheater bias is measured and shown in Supplementary Figure 3d. The measurement can then be used as a lookup table for the loading of the normalized weights. The weight values in Supplementary Figure 3a-c are illustrated accordingly. Supplementary Figure 3e-f shows the process of photodetection, which sums up all three weighted modulations, accomplishing the calculation of the inner product of the input vector  $d$  and weight

vector  $w$ . It should be noted that the zero voltage level does not necessarily correspond to the minimum level of the baseband multilevel digital signal, as indicated in Supplementary Figure 3f.

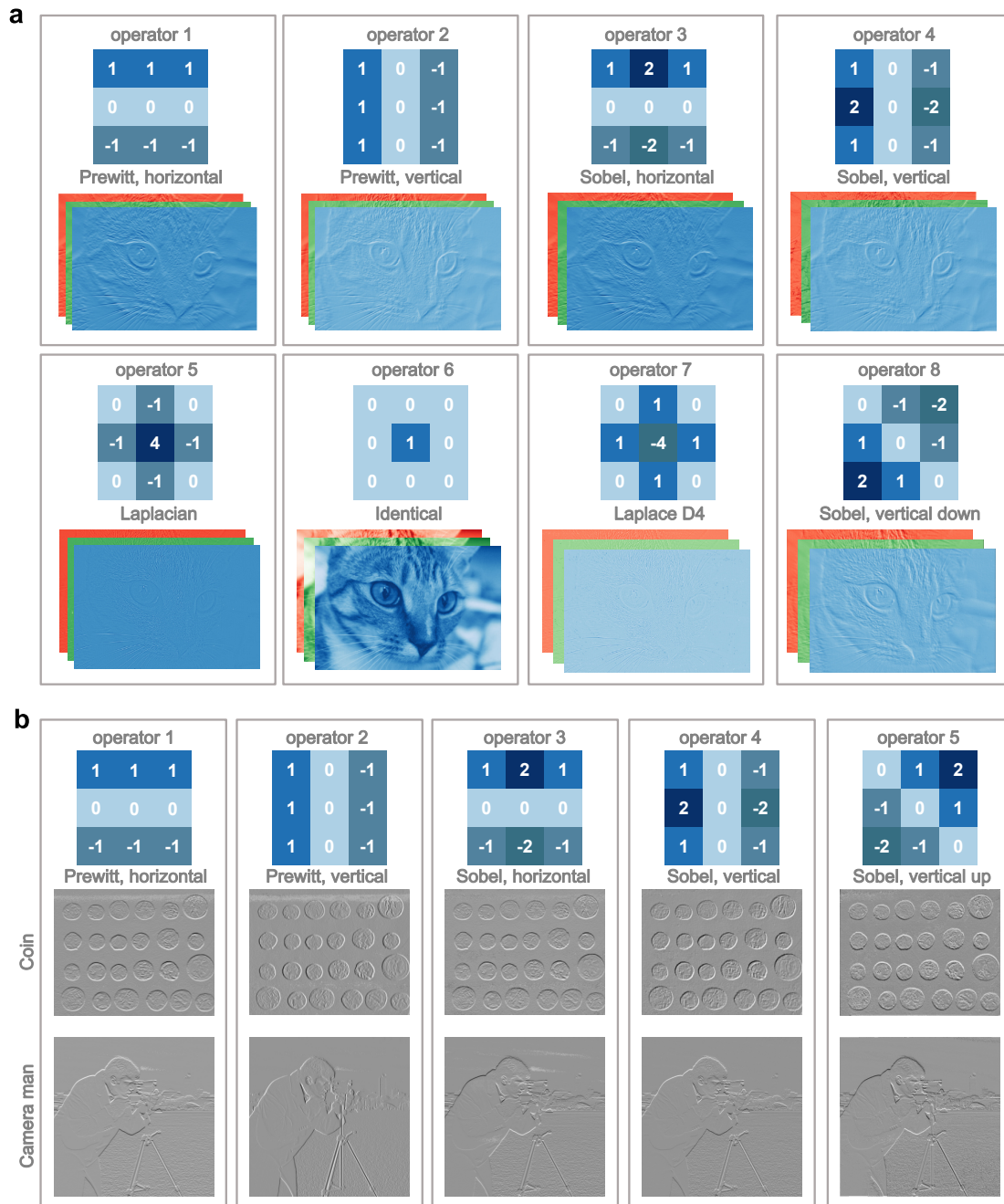
## 4 Convolution results from alternative operators and images

To further evaluate the performance of our HOP, we employed a variety of convolution operators and used alternative images. The convolution operators include Prewitt, Sobel, Sharpen D4, Identical, and Laplace D4. The convolutions are performed on an 8-bit image (Chelsea<sup>3</sup>) and the results are shown in Supplementary Figure 4a. Results from convolutions performed on alternative images in scikit dataset<sup>3</sup> are shown in Supplementary Figure 4b. The results clearly show a consistent performance with a minimized number of noisy pixels, indicating a reliable calculation precision across all tested operators and images.

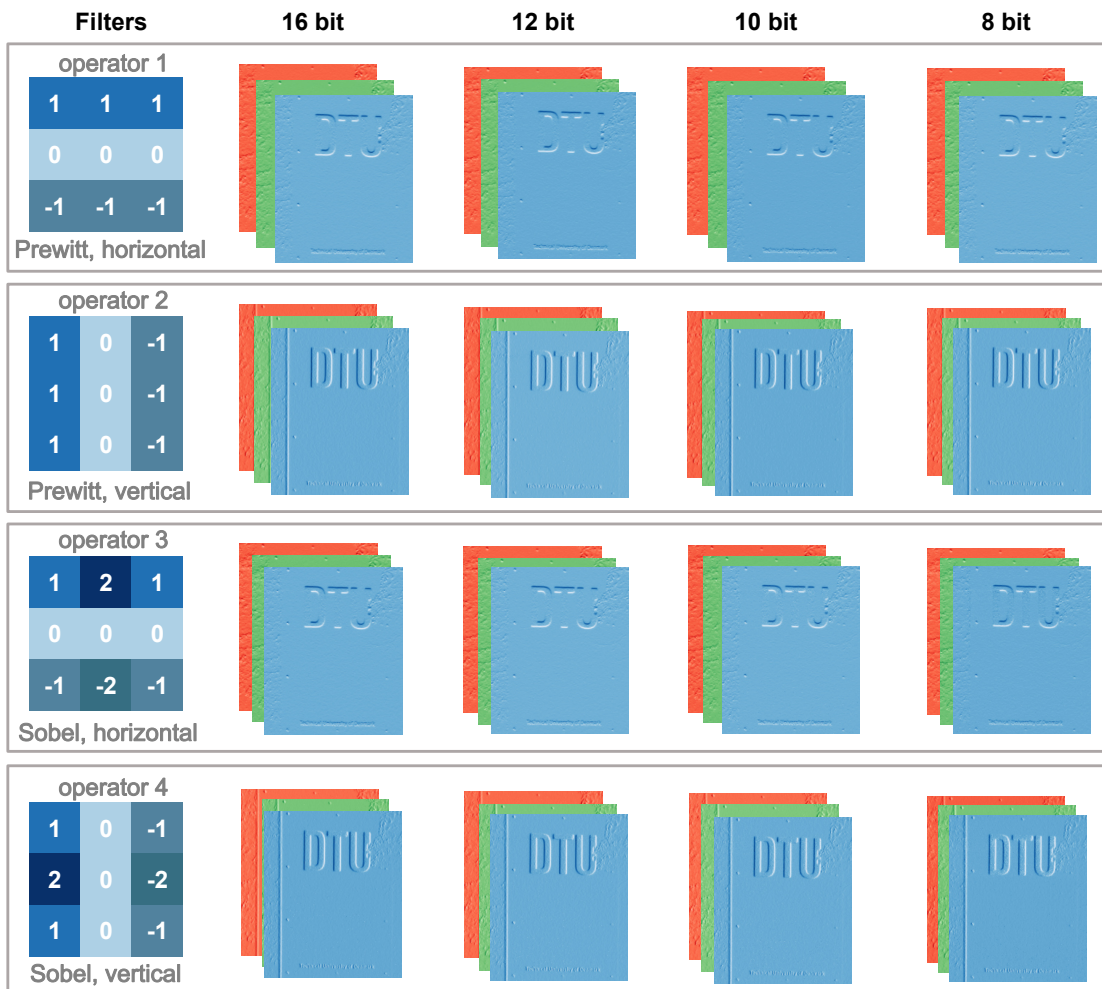
## 5 Convolution with variable bit precision

High bit-depth images are essential for some neural network applications. Higher bit-depths correspond to an increased number of possible color levels, thus enabling a richer display of color information. Many standards incorporate color depths of more than 8 bits, for example, 16-bit RAW, 12-bit Dolby Vision Standard (DVS), and 10-bit High Dynamic Range (HDR). An 8-bit Standard Dynamic Range (SDR) image offers  $2^8=256$  distinct color gradations, while a 16-bit image provides  $2^{16}=65536$  gradations.

To properly process such images without losing information, a calculation precision of 16 bits is required, and  $M = N = 16$ . Even for a small scale, i.e.,  $L = 9$  (for a  $3 \times 3$  convolution), the analog computing scheme requires DACs with 16-bit resolution and ADCs with 36-bit resolution (Eq. 1). While this might be possible, it is at the expense of a much slower ADCs conversion rate which then becomes a bottleneck. As previously discussed, for our HOP, the number of signal levels of the output and the resolution requirement for the ADCs do not depend on the precision of the input  $d$ . The HOP scheme eliminates the use of the DACs and requires ADCs with a much reduced resolution of 20 bits (Eq. 2), which is much more manageable and a significant improvement over analog computing schemes.



Supplementary Figure 4 | Alternative convolution results. **a**, Results using alternative convolution operators performed on an 8-bit image. **b**, Results performed on alternative images.



Supplementary Figure 5 | Convolution performed using variable bit precision.

Here, we demonstrate the capability of our HOP by processing an image with variable bit precision, using both Prewitt and Sobel operators on the same 16-bit image in the main paper, taken and preprocessed from a digital camera. The results are shown in Supplementary Figure 5. No performance difference is observed across images with different bit depths. This demonstrates that our HOP could indeed work with input values of any precision without sacrificing performance.

## 6 Scalability and system comparisons

Deep learning tasks usually require a greater number of convolution kernels and large matrix multiplication scales that are beyond the capability of current optical neural networks (ONNs). A large number of wavelength channels for the multi-wavelength light source together with massive hardware scaling for the photonic integrated circuit (PIC) is required. The multi-wavelength light source can be an optical frequency comb that provides more than a hundred wavelength channels and can be co-integrated to the PIC<sup>4</sup>.

The MRM based HOP has the advantage in terms of dimensions compared to Mach-Zehnder interferometer (MZI) based ONNs<sup>5</sup>. Envisioning a matrix multiplication task for  $64 \times 64$  matrices, 4096 MRMs are required for the HOP scheme. Taking into account the typical feature size ( $15 \mu\text{m}$  in diameter) and the pitch ( $30 \mu\text{m}$ ), the required chip size is estimated to be  $3.69 \text{ mm}^2$ , a size that is feasible for manufacturing. Achieving a high yield for a chip on this scale is very challenging. However, the MRM based HOP can introduce redundancies by implementing an excess number of MRMs for each convolution operator and an excess number of MRM arrays. Thanks to the nature of the MRMs, one down-performed MRM can be replaced by another MRM. And one MRM array can also be substituted by another array.

Simultaneously operating a large number of MRMs also presents a significant challenge, particularly due to discrepancies between design and manufacturing. It often requires correction by the microheater modulator to align the working wavelength of the MRMs to the multiwavelength light source, which could consume a significant amount of power. However, the post-fabrication trimming technique could solve this power consumption<sup>6</sup>.

Given the above discussion, the high noise tolerance of our HOP, the removal of DACs, and the relaxed resolution requirement for the ADCs, the MRM based HOP can be manufactured for

large-scale neural network applications.

Using achievable parameters for the photonic devices, we have compared our HOP with a state-of-the-art analog ONN processor<sup>7</sup> and Google’s tensor processing unit (TPU)<sup>8</sup> in terms of compute density (TOPS/mm<sup>2</sup>) and calculation precision. The results are shown in Supplementary Table 3.

The HOP scheme in this study operates at a clock speed of 7.5 GHz, processing matrices of size 3x3 and with a computing capacity of 8.44 GOPS. The effective area occupied by each MRM amounts to 900  $\mu\text{m}^2$ . The diameter of the ring is 15  $\mu\text{m}$ , and the pitch of the MRMs is 250  $\mu\text{m}$  in our fabricated chip, considering design redundancy<sup>9</sup>. Yet, the pitch could be reduced to 30  $\mu\text{m}$  or less if techniques such as undercut is used to manage thermal crosstalk<sup>10</sup>. This yields a compute density of 1.04 TOPS/mm<sup>2</sup>. The computing power can potentially be scaled up by increasing the operating speed to more than 40 GHz due to the elimination of DAC and relaxed resolution requirement for ADCs. As a result, the HOP can potentially achieve a compute density larger than 5.6 TOPS/mm<sup>2</sup>.

Evaluating the power consumption of the computing system requires knowledge of the power consumption from all supporting electronics, particularly the signal format converters (i.e., DACs and ADCs). However, this type of power consumption is often overlooked in the literature discussing analog ONNs. And it could depend on many factors such as the fabrication technology node. Therefore, we choose to eliminate the comparison of power consumption here. However, it should be noted the power consumption of our HOP can be much reduced compared with analog ONNs due to the removal of DACs and the relaxed resolution requirement for the ADCs. Nevertheless, the power consumption analysis for ONN lacks standards and should be investigated extensively in future research.

## References

- [1] Murmann, B. ADC Performance Survey 1997-2023. [Online]. Available: <https://github.com/bmurmann/ADC-survey>.
- [2] Redmon, J. & Farhadi, A. Yolov3: An incremental improvement. *arXiv preprint arXiv:1804.02767* (2018).
- [3] Van der Walt, S. *et al.* scikit-image: image processing in python. *PeerJ* **2**, e453 (2014).

Technology	Clock speed	Compute Density (TOPS/mm <sup>2</sup> )	Precision (bits)
Analog optical neural network <sup>7</sup>	12 GHz	1.2	5
Google TPU (ASIC) <sup>8</sup>	700 MHz	0.28	8
GPU(Nvidia H100 PCIe)	1.62 GHz	3.7	8
HOP	7.5 GHz	1.04 (3x3 matrix)	16
HOP	40 GHz	5.6 (64x64 matrix)	16

**Supplementary Table 3** | Performance comparison between different neural network processor schemes. Note that the computations here are fixed-point operations.

- [4] Jørgensen, A. A. *et al.* Petabit-per-second data transmission using a chip-scale microcomb ring resonator source. *Nature Photonics* **16**, 798–802 (2022).
- [5] Shen, Y. *et al.* Deep learning with coherent nanophotonic circuits. *Nature Photonics* **11**, 441–446 (2017).
- [6] Yu, X. *et al.* Ge ion implanted photonic devices and annealing for emerging applications. *Micromachines* **13** (2022). URL <https://www.mdpi.com/2072-666X/13/2/291>.
- [7] Feldmann, J. *et al.* Parallel convolutional processing using an integrated photonic tensor core. *Nature* **589**, 52–58 (2021).
- [8] Jouppi, N. P. *et al.* In-datacenter performance analysis of a tensor processing unit. In *Proceedings of the 44th annual international symposium on computer architecture*, 1–12 (2017).
- [9] Kong, D. *et al.* Intra-datacenter interconnects with a serialized silicon optical frequency comb modulator. *Journal of Lightwave Technology* **38**, 4677–4682 (2020).
- [10] Dong, P. *et al.* Low power and compact reconfigurable silicon multiplexing devices. In *Integrated Photonics Research, Silicon and Nanophotonics*, IWG5 (Optica Publishing Group, 2010).